The Effect of Particle Size on the Properties of (La,Sr)(Co,Fe)$O_{3-\delta}$ Ferrite-Based Cathodes for SOFCs

Charusporn Mongkolkachit and Suda Wanakitti
National Metal and Materials Technology Center
114 Paholyothin Rd., Klong 1, Klong Luang, Pathumthani, Thailand, 12120
E-mail: charuspm@mtec.or.th

Abstract

$La_{0.6}Sr_{0.4}Co_{0.2}Fe_{0.8}O_{3-\delta}$ (L60SCF) and $La_{0.56}Sr_{0.4}Co_{0.2}Fe_{0.8}O_{3-\delta}$ (L56SCF) cathodes for IT-SOFC application were prepared by solid state reaction. The mixture was calcined at 950 ˚C for 3 h. The perovskite materials were re-ground, sieved (using 140 and 325 mesh screens to get 2 particle size powders), then pressed into pellet shape at a pressure of 1 ton/cm^2 and sintered at 1100-1200 ˚C for 2 or 4 h. The preliminarily study of phase, particle size distribution, microstructure, density and thermal expansion coefficient were characterized. It was found that the smaller the particles, the less the energy and the lower sintering temperature required for sintering the samples. L56SCF with particle size of 0.37 μm achieved the lowest sintering temperature at 1100 ˚C for 2 h in this study. The sample showed single phase perovskite product with porous structure. The TEC of the sample was 14.5**5**×10^{-6} (˚C)$^{-1}$.

Keywords: Ferrite-based cathode, LSCF, Perovskite, IT-SOFCs

1. Introduction

Solid oxide fuel cell (SOFC) is a high efficiency and environmentally friendly technology. It is an electrochemical device that converts chemical energy into electrical energy. SOFC offers low emission level and high fuel flexibility. Recently, attention has been focused on lowering the operating temperature of SOFCs from 1000 ºC to an intermediate temperature range of 500-800 ºC. At this operating temperature, lower cost and more available materials such as stainless steels or other metallic materials could be used as interconnects, gas manifolds and heat exchangers. Such operating temperature enables use not only cheaper components, but also long-term stability materials and reduce the degradation of stack materials [1-2]. Two of the main considerations for an intermediate-temperature SOFCs (IT-SOFCs) are the increase in electrolyte resistance and high electrode overpotentials. The approaches to overcome these problems are; firstly, to use electrolyte with high ionic conductivity at low temperature range; secondly to reduce the electrolyte thickness; and thirdly to decrease the electrode polarization resistance [3-6].

In terms of cathode materials, this requires not only new cathode materials to be used, but also a new development of cathode microstructure [7]. The traditional LSM cathode material is a poor conductor at this intermediate operating temperature. A mixed electronic and ionic conductor, perovskite-type ABO_3 oxide, $La_{1-x}Sr_xCo_{0.2}Fe_{0.8}O_{3-\delta}$ system is one of the promising cathode materials for IT-SOFCs due to its high electrical and ionic conductivities.

Oxygen ionic conductivity is ascribed to the concentration of oxygen carrier (oxygen vacancy). The oxygen ion conductivity can be improved by the creation of more oxygen vacancies [8]. The cathode requirements for IT-SOFCs are sufficiently porous structure, high electrical conductivity, long-term stability and good compatibility with other components.

The purpose of this study was to investigate the thermal expansion coefficient, microstructure, phase and particle size distribution of prepared $La_{0.56}Sr_{0.4}Co_{0.2}Fe_{0.8}O_{3-\delta}$ (L56SCF) and $La_{0.6}Sr_{0.4}Co_{0.2}Fe_{0.8}O_{3-\delta}$ (L60SCF) cathode materials. It has been suggested that particle size has the major influence on the sintering condition affecting the performance of the prepared cathodes.

2. Experimental

$La_{0.56}Sr_{0.4}Co_{0.2}Fe_{0.8}O_{3-\delta}$ (L56SCF) and $La_{0.6}Sr_{0.4}Co_{0.2}Fe_{0.8}O_{3-\delta}$ (L60SCF) powders were prepared by the solid state reaction of La_2O_3 99.9%, $SrCO_3$ 99.9%, Co_3O_4 and Fe_2O_3 99%. The batch powders were ball milled for 15 h, dried and calcined at 950 ˚C for 3 h, then re-milled for 15 h to get a homogeneous mixture. The powders were divided into 2 parts and sieved using 140 (indicated as "part 1") and 325 mesh screens (indicated as "part 2"). Particle size distributions of prepared powders were examined. These powders were dry pressed into pellets at a pressure of 1 ton/cm^2. The selected pellets were sintered in air in the temperature range 1100-1200 ˚C for 2 or 4 h. The perovskite phase was analyzed by X-ray diffractometer (JEOL JDX-3530). Scanning electron microscope (SEM, JSM-5410) was used for microstructure analysis. Density of the samples was determined by Archimedes method. TEC was investigated by Anter Unitherm 1161 Dilatometer. Comparisons of the samples prepared from L56SCF, L60SCF and commercial $La_{0.6}Sr_{0.4}Co_{0.2}Fe_{0.8}O_{3-\delta}$ (commercial LSCF) [9] were examined.

3. Results and Discussion

3.1 Phase and Structural Study

An X-ray diffraction pattern for the calcined LSCF powders compared with the commercially available LSCF powder is shown in Figure 1. The single phase of rhombohedral perovskite structure was observed in all samples. The particle sizes of L60SCF ($La_{0.6}Sr_{0.4}Co_{0.2}Fe_{0.8}O_{3-\delta}$) powders indicated as "part 1" and "part 2" were 9.67 and 0.84 μm, respectively and those of L56SCF ($La_{0.56}Sr_{0.4}Co_{0.2}Fe_{0.8}O_{3-\delta}$) powders were 6.55 and 0.37 μm, respectively.

Figures 2 and 3 show the XRD spectra of each composition sintered at 1100 ˚C, 2 h and 1150 ˚C, 2 h, respectively. The results revealed the single phase product of perovskite structure. All sintered samples confirmed full conversion to the rhombohedral perovskite system.

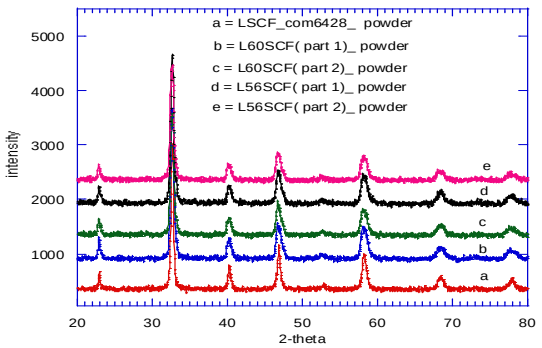

Fig. 1 XRD spectra for LSCF powders: (a) commercial LSCF powder; (b) calcined L60SCF powder (9.67 μm); (c) calcined L60SCF powder (0.84 μm); (d) calcined L56SCF powder (6.55 μm) and (e) calcined L56SCF powder (0.37 μm).

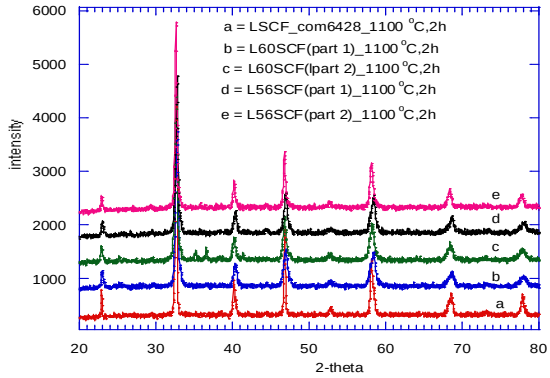

Fig. 2 XRD spectra for LSCF samples sintered at 1100 ˚C, 2 h: (a) commercial LSCF; (b) L60SCF (9.67 μm); (c) L60SCF (0.84 μm); (d) L56SCF (6.55 μm) and (e) L56SCF (0.37 μm).

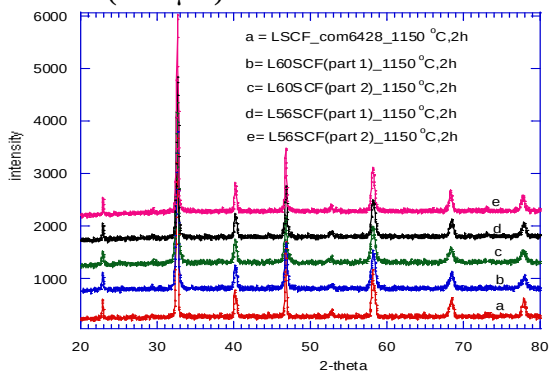

Fig. 3 XRD spectra for LSCF samples sintered at 1150 ˚C, 2 h: (a) commercial LSCF; (b) L60SCF (9.67 μm); (c) L60SCF (0.84 μm); (d) L56SCF (6.55 μm) and (e) L56SCF (0.37 μm).

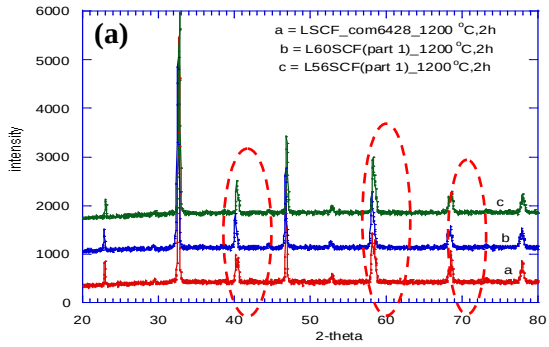

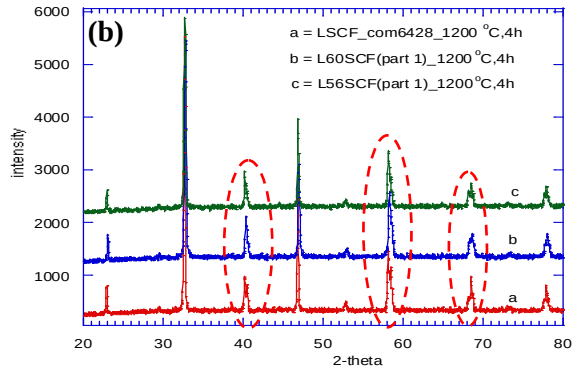

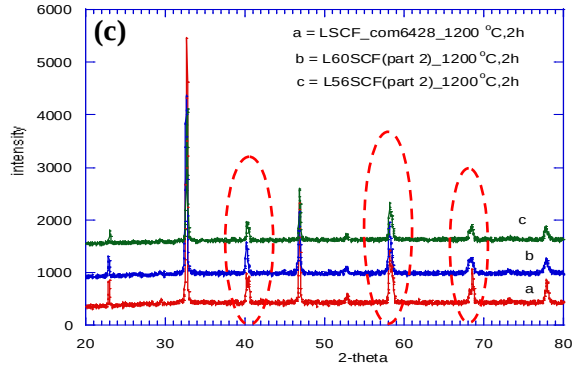

Fig. 4 XRD spectra for LSCF samples: (a) coarse powder samples sintered at 1200 ˚C, 2 h; (b) coarse powder samples sintered at 1200 ˚C, 4 h (c) fine powder samples sintered at 1200 ˚C, 2 h.

It was found that sintering temperature at 1200 ˚C was excessively high for this study (Figure 4). The splitting of the peaks at $2\theta \approx 40$, 58 and 68˚ appeared to be further away than that of lower sintering temperatures, obviously at $2\theta \approx 68$˚ (as indicated in the Figure). It is suggested that this is a result of the perovskite changing the symmetry from rhombohedral to orthorhombic [10]. From this study it is observed that the sintering time has a slight effect on peak splitting compared to the sintering temperature (as seen in Figures 4 (a) and (b)). The finer powder of the same composition showed less effect of XRD peak splitting (Figure 4 (c)).

Figures 5 to 7 show microstructure of various LSCF cathodes sintered at

different sintering conditions. Commercial LSCF sample hardly formed any sintering necks at 1100 ˚C, 2 h (Figure 5 (a)).

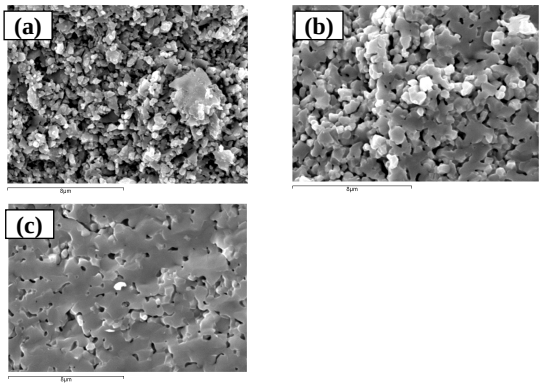

Fig. 5 SEM micrographs of commercial LSCF: (a) sintered at 1100 ˚C, 2 h; (b) sintered at 1150 ˚C, 2 h and (c) sintered at 1150 ˚C, 4 h.

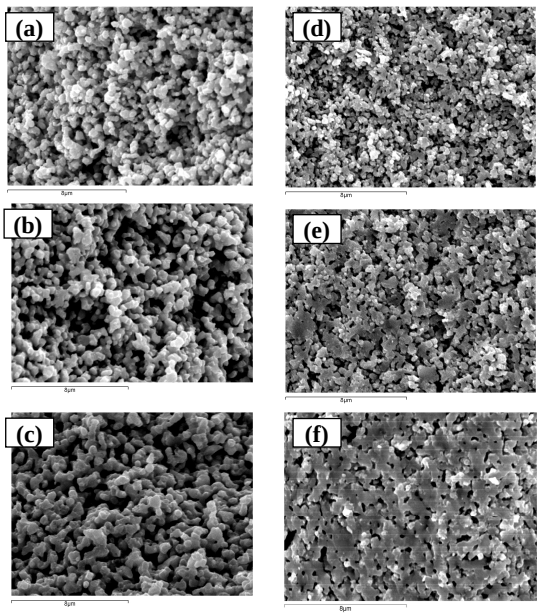

Fig. 6 SEM micrographs of L60SCF: (a) to (c) the coarse powder (9.67 μm) sintered at 1100 ˚C (2 h), 1150 ˚C (2 h) and 1150 ˚C (4 h), respectively; and (d) to (f) the fine powder (0.84 μm) sintered at 1100 ˚C (2 h), 1150 ˚C (2 h) and 1150 ˚C (4 h), respectively.

Figure 6 exhibits the porous structure of L60SCF. At higher sintering temperature, there were changes in particle morphology leading to particle coarsening and densification. At 1150 ˚C, the samples prepared from the finer powders (0.84 μm), Figures 6 (e) and (f), achieved the larger grain size and densified microstructure with sufficient porosity.

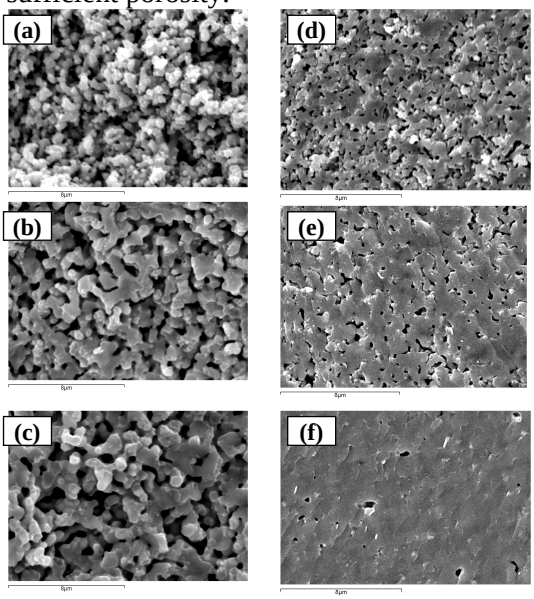

Fig. 7 SEM micrographs of L56SCF: (a) to (c) the coarse powder (6.55 μm) sintered at 1100 ˚C (2 h), 1150 ˚C (2 h) and 1150 ˚C (4 h), respectively; and (d) to (f) the fine powder (0.37 μm) sintered at 1100 ˚C (2 h), 1150 ˚C (2 h) and 1150 ˚C (4 h), respectively.

Similarly as seen in Figure 7, the microstructure of L56SCF prepared from the finer powders (0.37 μm), Figure 7 (d), sintered at 1100 ˚C for 2 h was porous and grains were in good contact with each other. Figure 7 (f) appeared to be over sintered. There was much less porosity which is not a desired microstructure for cathode materials.

3.2 Physical Analysis

Table 1 shows comparisons of particle size distribution of L56SCF and L60SCF powders. It was found that the particle size distribution of commercial LSCF powder was 0.64 μm and the smallest particle size

obtained in this study was 0.37 μm for the prepared L56SCF (sieved using a 325 mesh screen).

Table 1 Comparisons of particle size distribution of L60SCF and L56SCF powders.

Powder	Particle size (μm)	
	Part 1	Part 2
L60SCF	9.67±**0.**380	0.**84±0.0**12
L56SCF	6.55±**0.**390	0.**37±0.003**

Table 2 Bulk density of LSCF cathodes.

Sintering conditions	Bulk density (g/cm^3)				
	Commercial LSCF	L60SCF		L56SCF	
		Part**1***	Part**2**$^{\#}$	Part**1***	Part**2**$^{\#}$
1100 ˚C, 2h	4.42	3.08	4.22	3.22	5.02
1100 ˚C, 4h	4.85	3.07	4.42	3.31	5.14
1150 ˚C, 2h	5.51	3.65	4.86	4.05	5.65
1150 ˚C, 4h	5.78	4.15	5.24	4.52	5.73
1200 ˚C, 2h	6.01	5.34	5.71	5.51	6.00
1200 ˚C, 4h	6.09	5.56	N/A	5.72	N/A

Table 3 Apparent porosity of LSCF cathodes.

Sintering conditions	Apparent Porosity (%)				
	Commercial LSCF	L60SCF		L56SCF	
		Part**1***	Part**2**$^{\#}$	Part**1***	Part**2**$^{\#}$
1100 ˚C, 2h	27.65	49.96	31.31	47.23	17.75
1100 ˚C, 4h	20.81	49.65	28.24	45.46	15.84
1150 ˚C, 2h	10.91	40.83	21.56	34.18	5.45
1150 ˚C, 4h	3.91	33.71	15.03	26.60	3.96
1200 ˚C, 2h	0.41	14.48	6.33	9.36	0.62
1200 ˚C, 4h	0.47	10.19	N/A	4.91	N/A

Note: - Part 1* is powders with the particle size distribution of 9.67 and 6.55 μm for L60SCF and L56SCF, respectively.

- Part 2$^{\#}$ is powders with the particle size distribution of 0.84 and 0.37 μm for L60SCF and L56SCF, respectively.

- There was no data provided for 'Part 2' powder for 1200 ºC, 4 hr.

The bulk density and apparent porosity of LSCF samples prepared from various particle size powders and sintered at different sintering conditions are shown in Tables 2 and 3, respectively.

From Tables 2 and 3, the finer particle (Part 2) obtained higher bulk density with lower level of apparent porosity. For example the bulk density of L56SCF cathode (prepared from 0.37 μm powder) sintered at 1100 ˚C for 2 h is 5.02 g/cm^3 (17.75% apparent porosity), which is higher than that of commercial LSCF (4.42 g/cm^3, 27.65% apparent porosity) and prepared L60SCF (4.22 g/cm^3, 31.31% apparent porosity) sintered at the same condition. The higher bulk density, the lower apparent porosity showed in the samples. It is necessary to optimize between the bulk density (to obtain high green strength samples) and apparent porosity (to achieve porous microstructure and good contact between particles). It was found that the appropriate sintering condition that particles were in good contact with each other with porous microstructure for L56SCF (0.37 μm), commercial LSCF (0.64 μm) and L60SCF (0.84 μm) were 1100 ˚C (2 h), 1150 ˚C (2 h) and 1150 ˚C (**4** h), respectively. This was in good agreement with the particle size where the smallest particle (0.37 μm for L56SCF) required the lowest energy for the sintering process while the largest particle (0.84 μm for L60SCF) required the highest energy. The small particles with high surface area are easier to sinter and densify. Consequently, different particle sizes have different sintering properties. The optimum

apparent porosity contained in the sample should be high, approximately 30% [11, 12]. However, the level of apparent porosity for the fine powder (Part 2) in this study should be improved to achieve this value. To obtain the actual optimum sintering condition, these results have to be confirmed by the electrical property measurement.

Moreover, this was in coherent with the bulk density (Table 2) and apparent porosity (Table 3) of the samples. At the same sintering condition, the finer powders obtained the higher bulk density and lower level of apparent porosity. The decrease in porosity with increasing sintering temperature is owing to pore shrinkage or particle densification at high temperatures. The porosity reduces faster for the smaller particle sizes [13]. At elevated temperature, the coarsening of the particles occurred giving rise to a decrease in the porosity. Therefore the relatively low sintering temperature was chosen to achieve the porous structure. Consequently, the particle size has an effect on the sintering condition. The smaller the particles, the less energy and lower the sintering temperature required for the sintering process.

It has been expected that the structure of the cathode component has to be porous to allow oxygen ions to diffuse through the electrolyte. Over densified cathode could lead to low performance cathode materials.

3.3 Thermal Expansion Coefficient

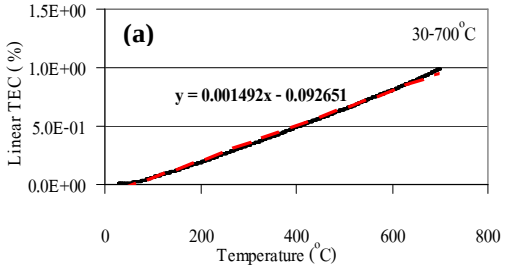

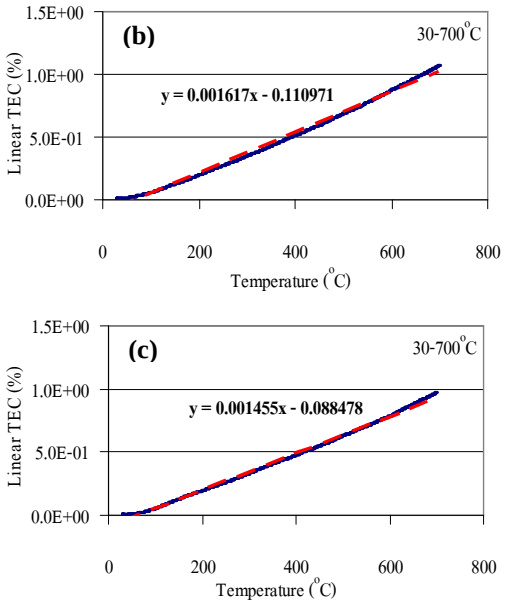

Fig. 8 TEC of LSCF cathodes in the temperature range 30-700˚C: (a) commercial LSCF, (b) L60SCF and (c) L56SCF.

Figure 8 shows the TEC values of commercial LSCF, L60SCF and L56SCF cathodes were 14.92×10^{-6}, 16.17×10^{-6} and 14.55×10^{-6} $(^{\circ}C)^{-1}$ (30-700 ˚C), respectively. These values for commercial LSCF and L56SCF are considered to be compatible with the TEC of CGO electrolyte [12.5×10^{-6} $(^{\circ}C)^{-1}$] (within ±20% range). It was found that the TEC of $La_{0.6-z}Sr_{0.4}Co_{0.2}Fe_{0.8}O_{3-\delta}$ system reduced for z = 0.05, and slightly increased when z increased [14]. However, the TEC values of L60SCF were different from that of the commercial sample although they have the same chemical composition. It is assumed that the preparation process of each powder was different resulting in different homogeneity and uniformity of prepared powders.

Next steps for this study are to investigate the electrical property and its correlation to phase and microstructure. Preparation of cathode powders by a chemical route should also be carried out. More investigations will be reported at a later stage.

4. Conclusion

$La_{0.6}Sr_{0.4}Co_{0.2}Fe_{0.8}O_{3-\delta}$ (L60SCF) and $La_{0.56}Sr_{0.4}Co_{0.2}Fe_{0.8}O_{3-\delta}$ (L56SCF) were prepared by the solid state reaction. It has been anticipated that particle size has the major influence on the sintering condition affecting on the performance of the prepared cathodes.

The samples exhibited single-phase rhombohedral perovskite structure. The microstructure of all samples was similar while the average particle size was different. Preliminarily, it can be concluded that the particle size affected the sintering conditions of the samples. The larger the particle, the higher the sintering temperature required. On the other hand, the smaller the particle, the lower the sintering temperature needed. This is because the small particles with high surface area are easier to be sintered and densified resulting in a decrease in the porosity. Therefore, different particle sizes have different sintering properties.

In order to produce the finer particles and homogeneous composition, alternative techniques (e.g. co-precipitation, sol-gel route) could be used. However, porosity level of the prepared samples needed to be considered. Therefore optimization of the sintering condition to achieve the porous microstructure with good contact between grains is required.

5. Acknowledgement

The authors would like to thank National Metal and Materials Technology Center (MTEC) for financial support through the project fund MT-B-50-END-07-032-I.

6. References

[1] Mai A., Haanappel V. A. C., Uhlenbruck S., Tietz F. and Stöver D., Ferrite-Based Perovskites as Cathode Materials for Anode-Supported Solid Oxide Fuel Cells: Part I. Variation of Composition, Solid State Ionics, Vol. **176**, No. 15-16, pp. **1341-1350**, 2005.

[2] Murata K., Fukui T., Abe H., Naito M. and Nogi K., Morphology Control of La(Sr)Fe(Co)$O_{3-\delta}$ Cathodes for IT-SOFCs, J. Power Sources, Vol. **145**, No. 2, pp. **257-261**, **2005**.

[3] Jiang S. P., Leng Y. J., Chan S. H. and Khor K. A., Development of (La,Sr)MnO_3-Based Cathodes for Intermediate Temperature Solid Oxide Fuel Cells, Solid-state Lett., Vol. 6, pp. A67-A70, 2003.

[4] Murray E. P., Sever M. J. and Barnett S. A., Electrochemical Performance of (La,Sr)(Co,Fe)O_3-(Ce,Gd)O_3 Composite Cathodes, Solid State Ionics, Vol. 148, No.1-2, pp. 27-34, 2002.

[5] Xia C. and Liu M., Novel Cathodes for Low-Temperature Solid Oxide Fuel Cells, Adv. Mater., Vol. 14, No. 7, pp. 521-523, 2002.

[6] Leng Y. J., Chan S. H., Jiang S. P. and Khor K. A., Low-Temperature SOFC with Thin Film GDC Electrolyte Prepared in Situ by Solid-State Reaction, Solid State Ionics, Vol. 170, No. 1-2, pp. 9-15, 2004.

[7] Hwang H. J., Moon J.-W., Lee S. and Lee E. A., Electrochemical Performance of LSCF-Based Composite Cathodes for Intermediate Temperature SOFCs, J. Power Sources, Vol. **145**, No. 2, pp. **243-248**, 2005.

[8] Kostogloudis G. C. and Ftikos C., Properties of A-Site-Deficient $La_{0.6}Sr_{0.4}Co_{0.2}Fe_{0.8}O_{3-\delta}$-Based Perovskite Oxides, Solid State Ionics, Vol. **126**, No. 1-2, pp. **143-151**, 1999.

[9] www.fuelcellmaterials.com.

[10] Waller D., Lane J. A., Kilner J.A. and Steele B. C. H., The Structure of and Reaction of A-Site Deficient $La_{0.6}Sr_{0.4-x}Co_{0.2}Fe_{0.8}O_{3-\delta}$ Perovskites, Mater. Lett, Vol. **27**, pp. **225-228**, **1996**.

[11] Liu Z., Ham M.-F. and Miao W.-T., Preparation and Characterization of

Graded Cathode $La_{0.6}Sr_{0.4-x}Co_{0.2}Fe_{0.8}O_{3-\delta}$, J. Power Sources, Vol. 173, No. 2, pp. 837-841, 2007.

[12] Büchler O., Serra J. M., Meulenberg W. A., Sebold D., Buchkremer H. P., Preparation and Properties of Thin $La_{1-x}Sr_xCo_{1-y}Fe_yO_{3-\delta}$ Perovskitic Membranes Supported on Tailored Ceramic Substrates, Solid State Ionics, Vol. 178, No. 1-2, pp. 91-99, 2007.

[13] Bissett H., Zah J., Krieg H. M., Manufacture and Optimization of Tubular Ceramic Membrane Supports, Powder Technol., Vol. 181, No. 1, pp. 57-66, 2008.

[14] Kostogloudis G. C. and Ftikos C., Properties of A-Site-Deficient $La_{0.6}Sr_{0.4}Co_{0.2}Fe_{0.8}O_{3-\delta}$-Based Perovskite Oxides, Solid State Ionics, Vol. **126**, No. 1-2, pp. **143-151**, 1999.